Science of the Total Environment 565 (2016) 922–932

Contents lists available at ScienceDirect

Science of the Total Environment

journal homepage: www.elsevier.com/locate/scitotenv

Process-generated nanoparticles from ceramic tile sintering: Emissions, exposure and environmental release

A.S. Fonseca [a,b,*], A. Maragkidou [c], M. Viana [a], X. Querol [a], K. Hämeri [c], I. de Francisco [d], C. Estepa [d], C. Borrell [d], V. Lennikov [d], G.F. de la Fuente [d]

[a] Institute of Environmental Assessment and Water Research (IDÆA-CSIC), C/ Jordi Girona 18, 08034 Barcelona, Spain
[b] Universidad de Barcelona, Facultad de Química, Martí i Franquès 1-11, 08028 Barcelona, Spain
[c] University of Helsinki, Department of Physics, Division of Atmospheric Sciences, P.O. Box 48, (Erik Palmenin aukio 1, Dynamicum), FI-00014, Finland
[d] Instituto de Ciencia de Materiales de Aragón (ICMA - Universidad de Zaragoza), María de Luna 3, E-50018 Zaragoza, Spain

HIGHLIGHTS

- Particle emissions and impact on worker exposure and the environment were assessed
- Nucleation processes were detected during thermal treatment
- Nanoparticles were emitted into workplace on a statistically significant level
- Workers exposure concentrations would exceed the recommended exposure limits
- A potential risk of nanoparticle release to the outdoor air was identified

GRAPHICAL ABSTRACT

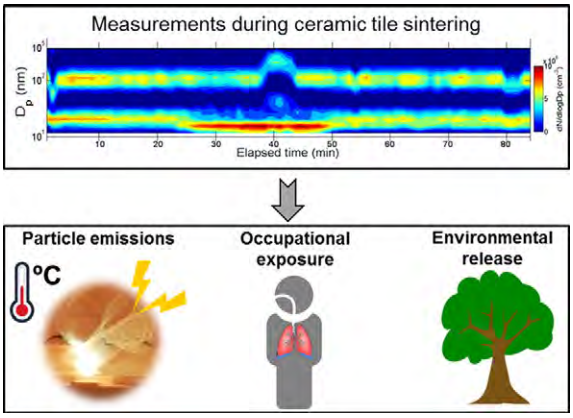

ARTICLE INFO

Article history:
Received 3 December 2015
Received in revised form 15 January 2016
Accepted 18 January 2016
Available online 2 February 2016

Keywords:
Occupational exposure
Industrial laser furnace
New particle formation
Particle transport
Indoor air
Ultrafine particles

ABSTRACT

The ceramic industry is an industrial sector in need of significant process changes, which may benefit from innovative technologies such as laser sintering of ceramic tiles. Such innovations result in a considerable research gap within exposure assessment studies for process-generated ultrafine and nanoparticles. This study addresses this issue aiming to characterise particle formation, release mechanisms and their impact on personal exposure during a tile sintering activity in an industrial-scale pilot plant, as a follow-up of a previous study in a laboratory-scale plant. In addition, possible particle transformations in the exhaust system, the potential for particle release to the outdoor environment, and the effectiveness of the filtration system were also assessed. For this purpose, a tiered measurement strategy was conducted.

The main findings evidence that nanoparticle emission patterns were strongly linked to temperature and tile chemical composition, and mainly independent of the laser treatment. Also, new particle formation (from gaseous precursors) events were detected, with nanoparticles <30 nm in diameter being formed during the thermal treatment. In addition, ultrafine and nano-sized airborne particles were generated and emitted into workplace air during sintering process on a statistically significant level. These results evidence the risk of occupational exposure to ultrafine and nanoparticles during tile sintering activity since workers would be exposed to

* Corresponding author at: C/ Jordi Girona 18, 08034 Barcelona, Spain.
E-mail address: ana.godinho@idaea.csic.es (A.S. Fonseca).

http://dx.doi.org/10.1016/j.scitotenv.2016.01.106

concentrations above the nano reference value (NRV; 4×10^4 cm^{-3}), with 8-hour time weighted average concentrations in the range of 1.4×10^5 cm^{-3} and 5.3×10^5 cm^{-3}.
A potential risk for nanoparticle and ultrafine particle release to the environment was also identified, despite the fact that the efficiency of the filtration system was successfully tested and evidenced a >87% efficiency in particle number concentrations removal.

1. Introduction

According to the Ceramic Industry Roadmap to 2050 (Cerame-Unie, 2012) by the European ceramic industry association, the European ceramic industry employs over 200 000 people in the EU-27, around 80% of them in small and medium-sized enterprises (SMEs). Ceramic manufacturing from the EU-27 Member States accounts for 23% of global production of ceramics. Ceramic manufacturing is, thus, considered a robust industrial activity at the global scale. It is also a growing industrial sector, which has benefited from advances made available through nanotechnology and through innovative industrial processes. However, processes applied in ceramic industries where heating or combustion are involved or where electrical and high energy equipments are used, such as the case of firing of the ceramics in kilns (Voliotis et al., 2014), laser tile sintering (Fonseca et al., 2015), or fracturing and abrasion activities (Fonseca et al., 2015), have evidenced that large ultrafine particle concentrations may be released to the workplace environment (up to 10^5 cm^{-3}) and that these particles may have potentially harmful mean diameters (<100 nm, ultrafine and <50 nm nanoparticles). The materials and the technology used may thus be significant sources of process-generated ultrafine and nanoparticles which may impact worker exposure.

The inhalation pathway is considered the predominant route of workplace exposure and uptake (Schmoll et al., 2009; Hansen, 2009). As particles reach smaller diameters they can travel deeper into the lungs (Oberdorster, 2001; Hoet et al., 2004; Heal et al., 2012; Weichenthal, 2012). The health outcomes of exposure to ceramic dusts are chronic obstructive pulmonary disease, reduced lung and respiratory symptoms such as risks of wheezing and breathlessness, dry cough and chronic bronchitis (Trethowan et al., 1995; Jaakkola et al., 2011; Kargar et al., 2013). Therefore, there is a need to characterise ultrafine and nanoparticle release mechanisms in these workplace settings similarly to what is done in industries dealing with engineered nanoparticles, in order to decrease workers exposure (Hameri et al., 2009; Van Broekhuizen, 2012; SER, 2012). However, exposure assessment studies for process-generated ultrafine and nanoparticles, especially as a result of innovations in the manufacturing processes, have received little attention in the scientific literature. Laser sintering of ceramic tiles is an innovative technique with a large potential for global-scale implementation in real-world ceramic industrial facilities. Laser sintering of tiles has numerous advantages such as speed, temperature and enhanced durability and surface properties of structural materials (de Francisco et al., 2011; Lahoz et al., 2011).

In this framework, this study addresses this knowledge gap by characterising particle release mechanisms and their impact on personal exposure during a tile sintering process using a high power CO_2 laser. As a follow-up to a previous study (Fonseca et al., 2015), the present work aims to identify and characterise nanoparticle formation and release mechanisms, as well as their impact on exposure, during the next step of the industrial up-scaling process in a 7 m-long industrial furnace (as opposed to a 3 m-long laboratory scale one) and in a facility emulating industrial-scale manufacture (as opposed to laboratory conditions). In addition, these industrial pilot-plant conditions allowed for the study of possible particle transformations in the exhaust system, the potential for particle release to the outdoor environment, and the effectiveness of mitigation strategies (such as the filtration system) already in place in the pilot plant.

2. Materials and methods

2.1. Measurement strategy

Aerosol measurements were conducted over six consecutive days in January 2015 in an industrial pilot plant scale furnace (length = 7 m) during a laser-based tile sintering process at the Instituto de Ciencia de Materiales de Aragón (ICMA) located in Zaragoza, Spain. It makes use of a 2000 W Rofin DC 025 SLAB CO_2 laser, equipped with the galvanic scan mirrors head emitting at a wavelength $\lambda = 10.6$ μm and an optical beam steering system (Estepa and de la Fuente, 2006; de Francisco et al., 2011). While the furnace applies heat to the tiles in the conventional sense, the laser is applied to the surface in order to reach higher temperatures which provide enhanced surface properties (Larrea et al., 2002; Mora et al., 2003; Lennikov et al., 2004, 2007, 2010; Estepa and de la Fuente, 2006; Gutiérrez Mora et al., 2009; de Francisco et al., 2011; Fonseca et al., 2015).

The main differences between the laboratory-scale furnace and industrial-scale furnaces should be highlighted here regarding the used fuel, gas flow and furnace length:

i. *Fuel*: industrial furnaces are powered by gas, as opposed to electricity in the case of the laboratory-scale furnaces.
ii. *Gas flow*: because of the different fuel used, the gas flow inside the industrial-scale furnaces is much higher than in laboratory-scale furnaces, and therefore, particle release to workplace air is expected to be lower.
iii. *Length*: industrial-scale facilities are frequently larger in length size and thus, lower particle concentrations at the breathing zone are expected, mainly due to the largest distances between the emission source and the breathing zone.

Based on these differences it seems acceptable to conclude that it is not possible to directly extrapolate the results regarding particle emissions obtained in the laboratory-scale furnace to the industrial-scale ones. In this work, the emissions from the furnace running were not included as they are considered negligible. The industrial furnaces usually are operated with gas, but in case of the present work an electrical furnace was used and therefore no emissions from the fuel are generated. Hence, the particle emissions are generated by the ceramic tile processing.

For the experimental procedure 6 of the most frequently used types of tiles in the ceramic industry were selected: red clay raw (#1), red clay raw with frit (#2), red clay raw with frit and decoration (#3), raw porcelain (#4), raw porcelain with frit (#5) and raw porcelain with frit and decoration (#6). The tile samples were 20 × 30 cm in size. Three replicas for each material were analysed. The tiles were introduced in the furnace at a constant velocity (8 m h^{-1}) in an orthogonal direction to the laser focus, and were gradually externally heated from ambient temperature up to 1000 °C and 950 °C for porcelain and red clay tiles, respectively. Upon reaching the peak temperatures, the laser beam was introduced and directed through an optical beam steering system, which transformed the circular cross-section beam into a line measuring 1 mm in thickness.

The methodology employed in this study followed the tiered measurement strategy described by various authors (Methner et al., 2010; VCI et al., 2011; Ramachandran et al., 2011; Asbach et al., 2012; Brouwer

et al., 2012) and follow the new harmonized tiered approach published by The Organisation for Economic Co-operation and Development (OECD, 2015). The measurement methods employed in this study aimed to study particles in the range 5 nm–20 μm and can be classified as online (size resolved/integrated and time resolved) and offline (size and time integrated) as follows:

- An electrical mobility spectrometer (NanoScan, SMPS TSI Model 3910; sample flow rate 0.7 L min^{-1}) to measure the particle mobility size distribution in 13 channels from 10 to 420 nm mobility diameter with a time resolution of 1 min.
- Miniature diffusion size classifiers DiscMini Matter Aerosol to measure total particle number, mean particle diameter, alveolar lung deposited surface area (LDSA) concentration as well as particles with a mode diameter between 10 and 700 nm. The sample flow rate and the sampling time interval were 1 L min^{-1} and 1 min, respectively.
- An optical particle counter (OPC, Grimm Model 1.108) to measure particle mass in the range 0.3 to 20 μm. The sample flow rate and the sampling time interval were 1.2 L min^{-1} and 1 min, respectively. The particles were classified in 15 channels according to their optical diameter.
- Particles collected on 25 mm polycarbonate filters with 0.8 μm pore size (one sample per ceramic material) for chemical analysis. Samples were gathered using cassettes (SKC Inc., inlet diameter 1/8 in.) connected to SKC Leland Legacy pumps operating at 6 L min^{-1}.
- Particle collection for chemical and morphological analysis by TEM (Jeol, JEM 1220, Tokyo, Japan), coupled with an energy-dispersive X-ray (EDX) spectroscopy were collected onto Quantifoil® Au grids with 1 μm diameter holes–4 μm separation of 200-mesh. TEM-grids were attached to air sample cassettes (SKC Inc., USA, inlet diameter 1/8 in. and filter diameter 25 mm). Air flow was driven by pumps operating at 6 L min^{-1} and collection efficiency for particles was assumed to be 100%.

All the filters were acid digested by using nitric acid (HNO_3), hydrofluoric acid (HF) and perchloric acid ($HClO_4$) following the method proposed by Querol et al. (2001) for the analysis of major and trace elements by ICP-AES (IRIS Advantage TJA Solutions, THERMO) and ICP-MS (X Series II, THERMO). Laboratory blank filters were analysed following the same methodology. Element concentrations were blank corrected.

The particle monitors and samplers were placed simultaneously at the emission source (furnace), in the worker breathing zone (BZ). In addition, three locations along the exhaust tube connecting the emission source to outdoor air were also assessed: (i) immediately above the laser chamber, (ii) before the high-efficiency particulate air (HEPA) filter and (iii) after the HEPA filtering system, immediately before the exhaust to outdoors (at 50 cm from outdoor air).

The worker area, where the workers operated the furnace control, was located approximately 1.5 m from the furnace. The sampling tube inlets were placed at the height of the breathing zone of the workers (Brouwer et al., 2009). The work environment showing the instrumentation and sampling locations are shown in Fig. 1.

Background particle concentrations (particles infiltrated from outdoors or other work-related activity occurred in parallel to tile sintering process) may be considered significant at lower concentration in the workplace and hence crucial to take into account in exposure assessment studies (Kaminski et al., 2015). In this particular study, the background was identified by using a time series approach during the non-activity period (measured at the breathing zone without the process of tile siltering in operation) before activity (Brouwer et al., 2009). This approach assumed that the concentration at the working area corresponds to the background and any increase in particle concentrations during the work activity is related to the working process itself (Kaminski et al., 2015). However, it is important to take into consideration that this approach assumes background concentrations to be constant and possible temporal and spatial changes in the background are not considered. The use of a combined approach of time series and spatial analysis such as described by Kaminski et al. (2015) would allow the background distinction over a full shift period and hence, the estimation of the so called "*theoretical background*". However, besides the measurement location at the work area, a second measurement location would be necessary to calculate the background particle concentration in the work area during the work activities. Because tile sintering was the only activity in the plant during this work it was considered not essential to account for the possible temporal and spatial changes in the background.

2.2. Data quality

The use of different instruments monitoring similar parameters at different sampling locations aimed to maximize the number of valid data points obtained, given that the risk of exceeding the measurement ranges of the instruments was high (due to the high nanoparticle emissions expected, Fonseca et al., 2015). This was the case of DiscMini and the NanoScan instruments placed in parallel at the emission source, to monitor particle number concentrations (N) although in different size ranges. For this reason, in the results and discussion section only one of the datasets will be discussed for each parameter. In the case of total N and for the mean particle diameter (D_p), the results presented will be those obtained with the DiscMini data, because it is the only instrument for which particle diameter data were available simultaneously in the emission source and breathing zone. However, concerning the representative particle number size distributions of the released emissions, the NanoScan data will be used.

The particle mass concentration (PM_{10}, $PM_{2.5}$ and PM_1) values monitored with the Grimm monitor were previously calibrated with a collocated EU-reference high-volume sampler with a $PM_{2.5}$ cutoff inlet. $PM_{2.5}$ and PM_{10} were the only parameters for which an equivalent to an EU reference instrument was available, given that the rest of the parameters are unregulated (Viana et al., 2015). In the case of N, one of the DiscMini units was taken as internal reference for the correction of the others employed. The performance of these instruments was assessed with ambient air side by side prior the sampling campaign in terms of mean D_p and total N. Figs. S1 and S2 in Supplementary data show the regression analysis for the total N and mean D_p measured with NanoScan and DiscMini 2–DiscMini 4 compared with DiscMini 1 (reference) based on 1-min resolution data for 12 h intercomparison. The black line in each of these figures indicates the linear fit to the data points. The corresponding equations and correlation coefficients R^2 are also given in each graph. The intercomparisons evidenced a high degree of comparability in terms of total N concentration between the different instruments with correlation coefficients $R^2 > 0.96$. Different levels of agreement with DiscMini 1 (Reference) were registered with a slope on the order of 0.74–1.77, hence deviating at a maximum of 77%. Furthermore, the regression analysis obtained for NanoScan shows a higher y-intersect than the DiscMini 2–DiscMini 4 regressions mainly due to the lower particle size range measured (10–420 nm). The comparability for mean particle diameter was also reasonable with deviations <67% and with correlation coefficients R^2 in the range of 0.89–0.99.

2.3. Data processing

Workplace air particle concentrations deriving from process-generated particle emissions were calculated by using the similar approach described by Asbach et al. (2012) and Kaminski et al. (2015):

$$\text{Process-generated particle release} = WA - BG \quad (1)$$

where WA is the measured particle concentrations at the breathing zone during the work activity and BG is the background registered concentrations.

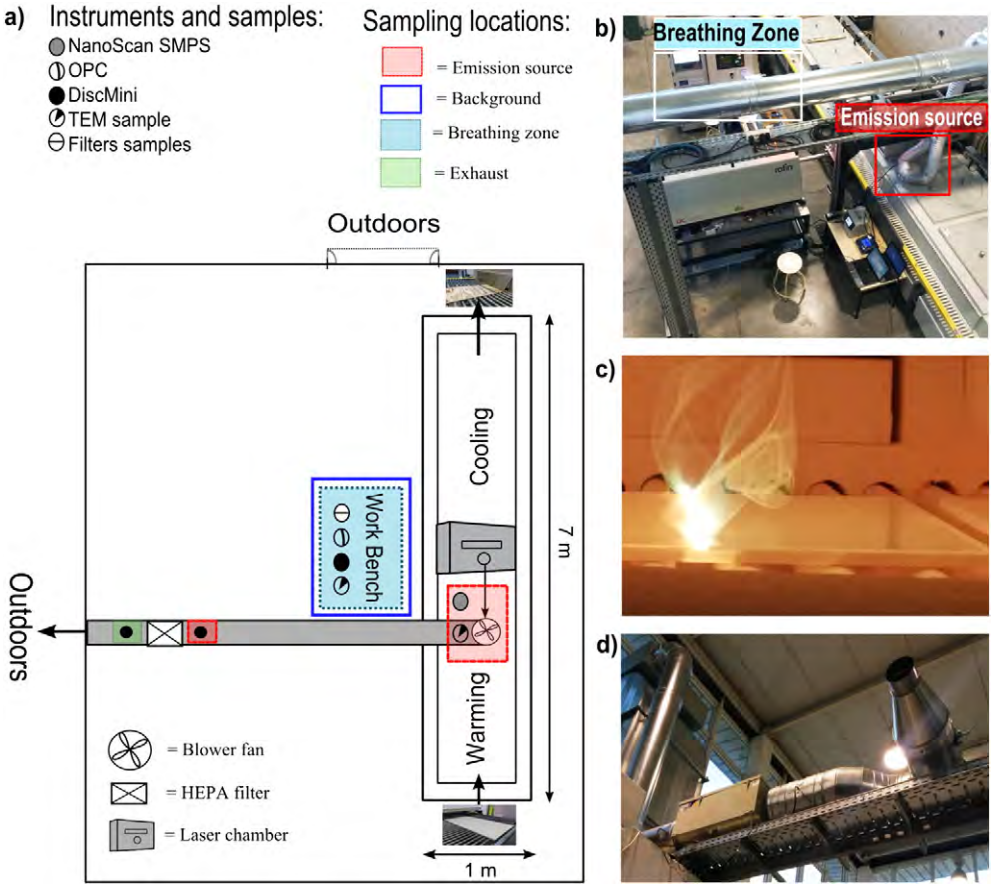

Fig. 1. Layout of the work environment. a) Approximate positions of processes and sampling locations; b) emission source and breathing zone; c) laser incidence on the tile surface, and d) HEPA filtering system.

According to Asbach et al. (2012), the process-generated particle release is statistically significant if the mean particle concentration in workplace air is higher than the *BG* concentrations plus three times the standard deviation ($3 \cdot \sigma_{BG}$) of the *BG* concentration. This means that if the ratio

$$\frac{\text{Process-generated particle release}}{3 \cdot \sigma_{BG}} > 1 \quad (2)$$

then particle release should be considered as significant.

The cumulative workers exposure for an 8-hour time weighted average (8 h TWA) was estimated as follows:

$$\text{Worker exposure}_{8\,\text{h TWA}} = \frac{t}{8\,\text{h}} \frac{1}{n} \sum_{i=1}^{n} WA_i \quad (3)$$

where, t is the time duration of the activity, WA_i is the measured background corrected particle concentration (subtracted the background concentration) and n is the total number of measurements.

In this study, an equivalent workers exposure of 7 h working shift during sintering activity with one specific ceramic material and 1 h working shift during non-activity period, was considered.

3. Results and discussion

3.1. Particle concentrations at the source

Fig. 2 summarises the median, mean, minimum, maximum and percentiles (P10, P25, P75 and P90) obtained at emission source in terms of number concentrations (range 10–700 nm), as well as the mean particle diameter emitted by each of the materials sintered (from #1 to #6) and for background air. Measurements were taken with 1 min time resolution, approximately 1.5 h in duration. Results are presented as average values for the number of replicas of each experiment carried out (data shown in supporting information, Figs. S3, S4 and S5.

As evidenced by Fig. 2, over the 1.5 h periods during which each of the tiles underwent the thermal treatment, major ultrafine and nanoparticle emissions reaching up to 1.0×10^7 cm^{-3} were registered at the emission source with mean diameters of 14 nm and 12 nm for red clay and porcelain tiles, respectively (Fig. 2). It can be observed that coarser particles (maximum diameters ranging between 28 and 30 nm) were detected during sintering of coated tile materials, independently of the base of the tile. On average, mean *N* minute concentrations were 2 orders of magnitude higher than background levels and the mean particle diameters were finer (10–16 nm) than in background air (58 nm). On average, mean nanoparticle emissions were moderately higher during porcelain sintering (2.3×10^6 cm^{-3}) than from red clay sintering (2.2×10^6 cm^{-3}). This finding is similar to the results from laboratory scale furnace (3 m long) (by measuring in the same range of 10–700 nm) where it was observed that red clay sintering emitted lower *N* (2.9×10^6 cm^{-3}) than porcelain sintering (5.0×10^6 cm^{-3}). Aside from this, it may be concluded that lower *N* were measured with the industrial-scale furnace when compared to the laboratory-scale one. Nonetheless, the conclusion is then that the larger furnace emits lower *N* than the laboratory scale furnace (Table 1).

Particle emissions from porcelain and red clay sintering showed similar mean diameters (12 ± 3 nm and 14 ± 5 nm, respectively), which were markedly finer than those from background air particles (58 ± 8 nm), influenced by vehicular traffic emissions (with a high percentage of diesel) in the surroundings of the pilot plant. These results are in agreement with those from the laboratory-scale furnace (Fonseca

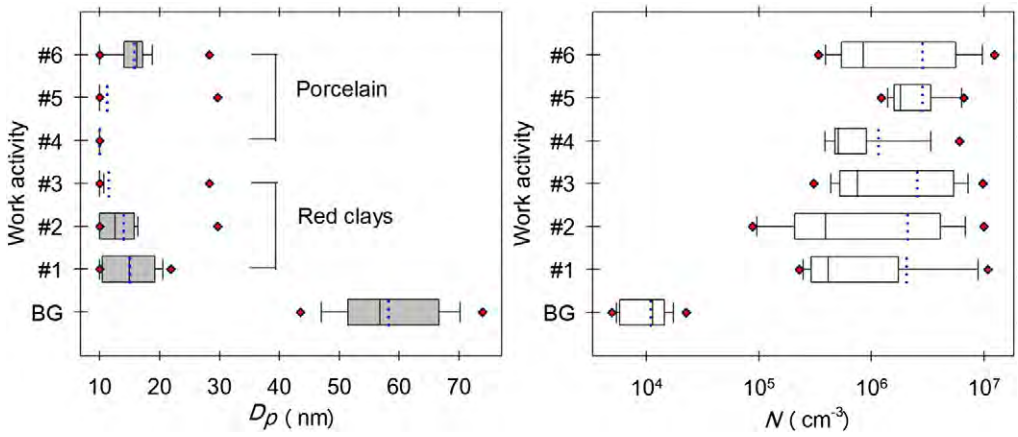

Fig. 2. Horizontal box plots for the tile sintering activity obtained at the emission source and background air with regard to mean particle diameter (D_p; DiscMini, range 10–700 nm) and particle number concentration (N; DiscMini, range 10–700 nm). The boundary of the box closest to zero indicates the 25th percentile, a line within the box marks the median, and the boundary of the box farthest from zero indicates the 75th percentile. Whiskers (error bars) above and below the box indicate the 90th and 10th percentiles. In addition, the mean is shown as dotted line and the outlying points as minimum and maximum (in red). Mean D_p was consistently < detection limit during the entire experiment of material #4 (raw porcelain).

et al., 2015), even if mean particle diameters were slightly different for the different materials then (16 ± 6 nm for red clay tiles and 10 ± 3 nm for porcelain, versus 34 ± 5 nm for background air). These results suggest that the size of the furnace does not have a major impact on the mean diameter of the particles emitted and, which is relatively dependent on the raw materials and coatings used.

As regards N, Table 1 shows that similar results were obtained across all the red clay tiles evaluated, independently of the presence or absence of coating materials (2.0×10^6 cm^{-3} for raw red clay, 2.1×10^6 cm^{-3} for red clay with coating and 2.5×10^6 cm^{-3} for red clay with coating and decoration). Conversely, with porcelain tiles, higher N were monitored with coated materials (2.8×10^6 cm^{-3}, Table 1) than with the raw tiles (1.1×10^6 cm^{-3}). These results were consistent across the different replicas tested. In both cases (red clay and porcelain), the highest mean N concentrations were recorded when sintering coated materials (with frit and/or decorated). These results suggest that nanoparticles may originate from the coating materials, as opposed to the base of tiles (with the exception of the raw red clay tiles).

3.2. Emission patterns

In order to understand the particle emission processes, the time series of N and D_p at the emission source are shown in Figs. 3, 5 and 6 (raw materials and one example of a coated material). The figures show the particle emission patterns as a function of the main parameters of the sintering process (temperature and incidence of the laser beam). The materials shown (raw red clay, raw porcelain, and porcelain coated with frit and decoration) were selected given that they are the most representative of the main emission patterns observed during tile sintering.

Fig. 3 shows the characteristic emission pattern observed for all coated materials, based on the example of porcelain with frit and decoration coating (material #6). Results show that when the tiles were externally heated in the furnace in a temperature range between 450 and 900 °C, constant N and relatively stable particle diameters (for 2 particle diameters, $15 < D_p < 37$ nm and $87 < D_p < 116$ nm) were monitored at the emission source and also impacting exposure in the breathing zone. Upon reaching the peak temperature in the furnace (900–1000 °C), a thermally-induced emission pattern was observed and a decrease in particle size for the smallest particles was detected (reaching minimum values of 10 nm or lower for all the coated materials). The particles with $87 < D_p < 116$ nm were not affected by this increase in temperature. It should be noted that the lower limit of detection of the particle sizing instruments (DiscMini and NanoScan) is 10 nm. As previously discussed by Fonseca et al. (2015), these results suggest the occurrence of new particle formation processes by nucleation (nanoparticles <30 nm in diameter being formed; Kulmala et al., 2004; Kumar et al., 2008) inside the furnace, which would result in higher N with a lower particle size. Nucleation processes from gaseous precursors were probably induced by the cooling down of exhaust gases containing SO_2 emitted from the thermal decomposition of S-bearing minerals present in the tile's raw material (e.g., anhydrite, $CaSO_4$, Fig. 4c and e), which decomposes at high temperatures (Chinchón et al., 1991). Upon introduction of the laser beam (still within the peak temperature stage), Fig. 3 shows a decrease in N and an increase in D_p (37 nm for the smallest particles as opposed to 10 nm during the thermal treatment), probably as a result of coagulation/condensation processes. This increase in size also affected the $87 < D_p < 116$ nm particles (increasing to 365 nm). Results seem to

Table 1
Mean and standard deviation (±σ) of particle number concentrations (N) and mean particle diameter measured during tile sintering (D_p; range 10–700 nm) at the emission source and in background air of the pilot plants (industrial-scale; laboratory-scale, Fonseca et al., 2015). Mean values (from #1 to #6) correspond to the average of the replicas analysed for each specific tile material, approximately 1.5 h in duration, each one. Mean D_p was consistently < detection limit during the entire experiment of material #4 (raw porcelain).

Material		Industrial-scale furnace (7 m)		Laboratory-scale furnace (3 m)*	
		N (cm^{-3})	D_p (nm)	N (cm^{-3})	D_p (nm)
Red clay tiles	#1	$2.0 \times 10^6 \pm 3.1 \times 10^6$	15.1 ± 4.1	$2.8 \times 10^6 \pm 4.1 \times 10^6$	15.9 ± 7.0
	#2	$2.1 \times 10^6 \pm 2.8 \times 10^6$	14.0 ± 4.8	$2.6 \times 10^6 \pm 5.2 \times 10^6$	17.9 ± 6.2
	#3	$2.5 \times 10^6 \pm 2.9 \times 10^6$	11.4 ± 4.7	$3.4 \times 10^6 \pm 6.1 \times 10^6$	14.5 ± 4.3
Porcelain tiles	#4	$1.1 \times 10^6 \pm 1.4 \times 10^6$	10.0 ± 0	$3.8 \times 10^6 \pm 5.1 \times 10^6$	8.0 ± 2.4
	#5	$2.8 \times 10^6 \pm 1.8 \times 10^6$	11.3 ± 4.7	$6.0 \times 10^6 \pm 3.6 \times 10^6$	10.9 ± 5.0
	#6	$2.8 \times 10^6 \pm 3.6 \times 10^6$	15.8 ± 3.9	$5.1 \times 10^6 \pm 4.0 \times 10^6$	10.5 ± 3.0
BG		$1.1 \times 10^4 \pm 4.7 \times 10^3$	58.2 ± 8.4	$1.3 \times 10^4 \pm 8.6 \times 10^3$	33.9 ± 5.5

* Fonseca et al. (2015).

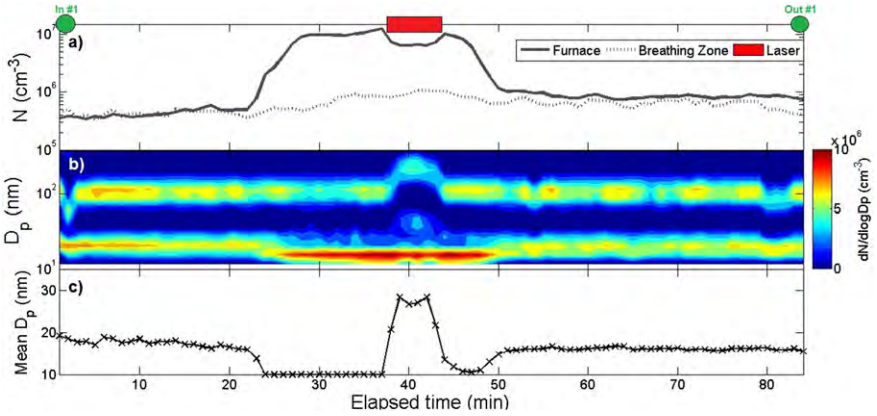

Fig. 3. Porcelain with frit and decoration coating (material #6). (a) Time series of (a) particle number concentrations (N) measured simultaneously at the emission source and the breathing zone (range 10–700 nm), and (b) particle size distributions (range of 10–420 nm), and (c) mean particle diameter (D_p) at the emission source (range 10–700 nm). The laser period is shown as red rectangle and the entrance and exit of material are shown as green circles. Results for one of the replicas analysed of the same material, representative of all the replicas.

suggest that the incidence of the laser inhibited further particle formation mechanisms, possibly due to the sealing of the tile's surface with the laser, and conversely favoured particle growth. Upon completion of the laser treatment, nucleation events were once again detected as a decrease in mean particle size down to 10 nm and an increase in N. During the cooling stage (temperatures decreasing to 800 °C), N dropped back to the initial concentrations and a significant particle growth was observed, probably due to condensation of gaseous species on pre-existing particles and/or the coagulation processes. As stated above, this pattern was observed for all coated materials (whether using red clay or porcelain as substrate; (Figs. S3, S4 and S5 in Supplementary data).

Fig. 4 shows examples of ultrafine and nanoparticle morphology and composition detected at the emission source during sintering activity. The TEM/EDX analyses of the samples show a large number of spherical ultrafine particles ranging from 10 nm–1000 nm in size diameter which may be interpreted as portions of melted material involved in the tile melting processes. In addition, a large amount of agglomerated particles were collected by TEM (Fig. 4a, d and f), thus confirming the occurrence of particle condensation and/or agglomeration of existing finer nanoparticles (10–30 nm in size diameter) from nucleation process.

Different emission patterns were registered when monitoring raw materials, which were in addition different for the two materials evaluated. Fig. 5 shows the case of raw red clay. The emission pattern observed during raw red clay sintering showed certain similarities with that described for coated materials (Fig. 3), showing lower N and larger diameters ($15 < D_p < 37$) during the lowest temperature stages and new particle formation processes by nucleation before and after the laser treatment coinciding with the highest temperatures inside the furnace (particle diameters <20 nm). The main difference with regard to the coated materials was found during the laser treatment, when particle diameters did not increase as much as in Fig. 3 (mean diameter during the laser treatment = 81 nm with coated materials vs. 43 nm with raw red clay). In addition, almost no emissions of larger-sized particles (around 100 nm) were detected from raw red clay sintering (Fig. 5), which points to the coating materials (and not the tile substrate) as their most probable source.

Finally, the emission pattern of raw porcelain sintering was also assessed (Fig. 6). A different pattern was observed on this occasion, which was replicated in all the analyses of raw porcelain carried out. As shown in Fig. 6, particle emissions followed similar trends as in the case of raw red clay, with only one dominant particle size (20 nm, as opposed to two particle sizes obtained with coated materials). However, upon incidence of the laser beam an increase in N was detected, while particle diameter showed a slight decrease (up to 10 nm). This result would suggest that, in contrast to all other materials, during sintering of raw porcelain nucleation events took place during the laser treatment.

To summarise, nucleation process (nanoparticles <30 nm in diameter being formed) were detected for both materials (red clay and

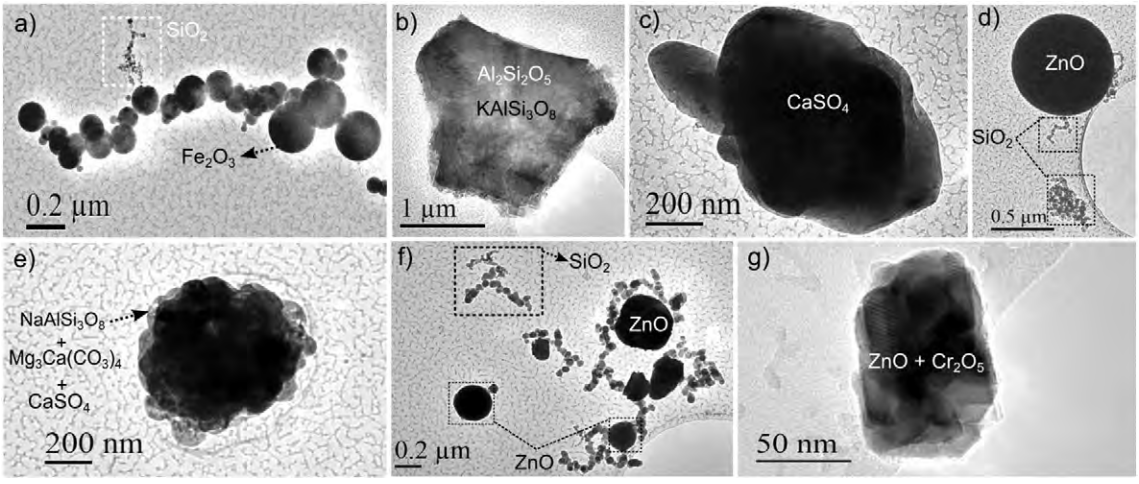

Fig. 4. TEM images of nanoparticles collected at the emission source during different sintering activities: a) red clay raw; b) red clay frit coated; c) and d) red clay frit and decoration coated; e) raw porcelain; f) porcelain frit coated and g) porcelain frit and decoration coated. Corresponding identified particles by TEM/EDX are shown in each figure.

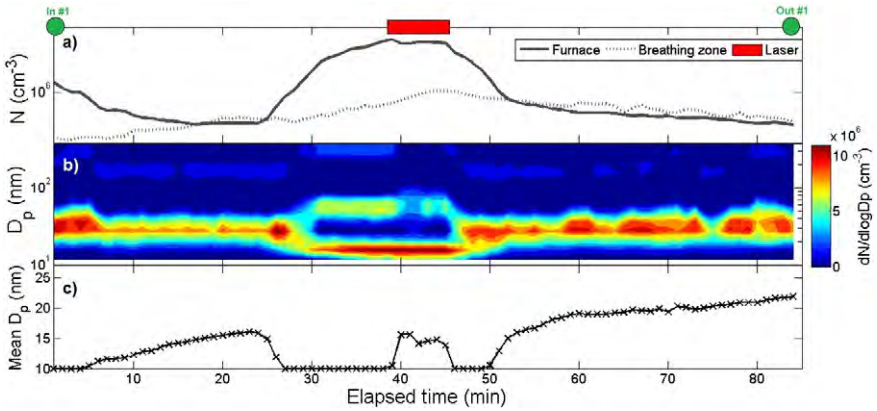

Fig. 5. Raw red clay (material #1). Time series of (a) particle number concentrations (N) measured simultaneously at the emission source and the breathing zone (range 10–700 nm), and (b) particle size distributions (range of 10–420 nm), and (c) mean particle diameter (D_p) at the emission source (range 10–700 nm). The laser period is show as red rectangle and the entrance and exit of material are shown as green circles.

porcelain) during the thermal treatment, independently of the laser treatment. This result goes beyond the results from the previous study (under laboratory conditions) where such events were only observed during red clay sintering. Except for the raw porcelain, the influence of the laser treatment results in the emission of larger particles than when compared to the same temperature (950–1000 °C) without the laser. This suggests that the incidence of the laser inhibits new particle formation processes by nucleation which can be observed immediately before the laser treatment.

3.3. Exposure to particles in the breathing zone

The particles emitted inside the furnace were released to workplace air and transported toward the worker area, resulting in potentially health-hazardous exposures for the workers. The mean N and D_p measured in the breathing zone for each of the materials analysed, as well as in background air, are presented in Fig. 7. A comparison with the results from the laboratory-scale furnace (3 m long, Fonseca et al., 2015) is also included.

As shown in Fig. 7, mean N in the breathing zone were in all cases at least 1 order of magnitude higher than background levels, thus confirming the increase in worker exposure to ultrafine and nanoparticles resulting from the sintering process. Regarding particle transport across the workplace, N in the breathing zone were much lower than in the emission source for all the materials, as expected (Figs. 2 and 7) due to dilution of the emissions in combination with particle agglomeration and coagulation. However, in all cases and similarly to previous laboratory-scale study, N were significantly above background concentrations since mean N in workplace air were always higher than the background concentrations plus three times the standard deviation of the background concentration ($>3.9 \times 10^4$ cm^{-3} and 2.5×10^4 cm^{-3} for particles in the range of 10–700 nm, at 3 m and 7 m furnace, respectively). As a result, the increase in worker exposure was considered statistically significant.

When comparing the results from the industrial-scale and the laboratory-scale pilot plants (Fonseca et al., 2015), results show that breathing zone N concentrations were lower for most materials in the laboratory-scale plant, with the exception of materials #1 and #2. The highest exposure concentrations were recorded during porcelain sintering (3.6×10^5 cm^{-3}), and more specifically for the porcelain with frit and decoration tiles (#6), reaching mean N of 6.2×10^5 cm^{-3}. The decrease in exposure concentrations when compared to the laboratory-scale conditions (Fig. 7) was probably related to the higher gas flow inside the industrial-scale furnace than in laboratory-scale one and also to the size of the facility (mainly, the distance between the emission source and the breathing zone). Particle diameters were lower in the industrial-scale plant due to their lower emission diameters.

Worker exposure during the sintering processes was also calculated in terms of particle mass (PM) (Fig. 8). As in the case of N, PM concentrations in the breathing zone were consistently higher than in background air. The maximum mean concentrations registered were 6.0 μg m^{-3}; 18 μg m^{-3} and 70 μg m^{-3} for PM_1, $PM_{2.5}$ and PM_{10}, respectively, for raw porcelain (material #4). The ratio (Eq. (2); Process-generated particle release/3 · σ_{BG}) results in 1.1, 2.7 and 7.8, respectively and thus

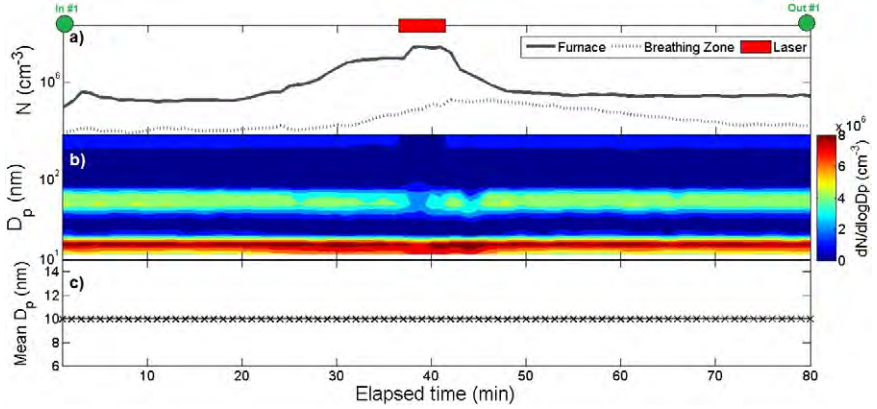

Fig. 6. Raw porcelain (material #4). Time series of (a) particle number concentrations (N) measured simultaneously at the emission source and the breathing zone (range 10–700 nm), and (b) particle size distributions (range of 10–420 nm), and (c) mean particle diameter (D_p) at the emission source (range 10–700 nm). The laser period is show as red rectangle and the entrance and exit of material are shown as green circles. Mean D_p (c) was consistently < detection limit during the entire experiment.

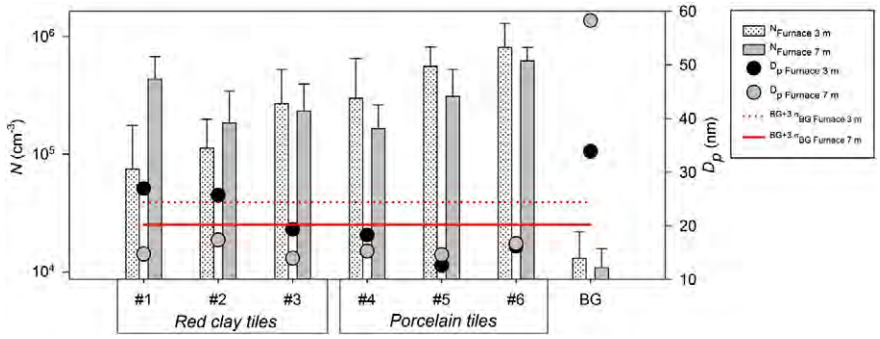

Fig. 7. Particle number concentrations (N) and mean particle diameter (D_p; range 10–700 nm) measured in the breathing zone for each of the materials analysed, as well as for background air. Mean values correspond to each sintering process, approximately 1.5 h. The left and right y-axis refer to the mean N and mean D_p, respectively. Error bars above the box indicate the standard deviation (σ). The solid and dashed red horizontal lines indicate the significance level of particle release during sintering activity in the workplace air in the pilot-plant (7 m) and laboratory-scale furnaces (3 m), respectively ($BG + 3 \cdot \sigma_{BG}$; Asbach et al., 2012).

should be considered a statistically significant increase in exposure concentrations, for this material (Asbach et al., 2012). For the rest of the materials, exposure was significantly high only for PM_{10} and for materials #1, #2, #5 and #6 (Fig. 8). This was likely caused by re-suspension of coarse particles which is commonly observed during activities in indoor environments (by walking, etc.). TEM/EDX analyses confirmed the presence of coarse particles (agglomerates, coarse size) in workplace air (Fig. 4a, d and f).

The results concerning the *PM* concentrations presented here are considerably higher than those found in laboratory scale. Fonseca et al. (2015) measured an average PM_{10} exposure during the same sintering activities varying from 12 to 17 μg m^{-3} whereas the results of PM_{10} presented here, showed levels of 7–70 μg m^{-3}, although not very high for a working place.

3.4. Particle characterisation

The conducted TEM/EDX analyses of the samples show that quartz (SiO_2) appears to be the main inorganic component released in both types of tiles. Other crystalline constituents found in both types of tiles were albite ($NaAlSi_3O_8$), metakaolinite ($Al_2Si_2O_5$), and huntite ($Mg_3Ca(CO_3)_4$). Conversely, mineral phases such as microcline ($KAlSi_3O_8$) and hematite, (Fe_2O_3) were only found in red clay tiles whereas augite ($CaMg(Fe, Al, Ti)(Si Al)_2O_6$ only in porcelain tiles. In addition, metal oxide nanoparticles of Zn, Cr, Al and Fe were also found, resulting from their use as opaque frits or pigments (Jacobs, 1954; Romero et al., 2003; Minguillon et al., 2009; de la Sánchez Campa et al., 2010; Lahoz et al., 2011; Casasola et al., 2012; Celades, 2013).

The chemical analysis of particles collected on 25 mm polycarbonate filters revealed also that a considerable amount of SO_4^{2-} (14–24% of total particle mass) was consistently found in workplace air (Fig. S6 in Supplementary data). Other relevant components found in both raw tiles were $CaCO_3$ and SiO_2 (6% of particle mass concentration, each). Commonly used in frit and decoration coated tiles, a relevant percentage of ZnO was found for both porcelain and red clay tiles (4% and 7% for red clay frit and decoration coated (material #3) and porcelain frit coated, respectively).

3.5. Comparison of worker exposure concentrations with the nano reference values

Although occupational exposure limits (OELs) were established by Council Directive 88/642/EEC as "*the limit of the time-weighted average of the concentration of a chemical agent in the air within the breathing zone of a worker in relation to a specified reference period*" (EC, 1998), no OELs are available regarding nanoparticles or nanomaterials yet. Despite this, nano reference values (NRVs) have been set by Social and Economic Council of The Netherlands (SER, 2012) regarding worker exposure to engineered nanoparticles (ENPs). NRVs are background-corrected 8-hour TWA concentrations. However, high-energy processes such as the pone under study may generate nanoparticle emissions to workplace air, which by nature are comparable to ENPs in terms of hazardous properties (Van Broekhuizen, 2012). According the SER (2012), for low-density biopersistent granular nanomaterials (density < 6000 kg m^{-3} such as Al_2O_3, SiO_2, ZnO, etc.) and for high-density biopersistent granular nanomaterials (density > 6×10^3 kg m^{-3}) such as Ag, Au, CeO_2, etc.), the NRVs are 4×10^4 cm^{-3} and 2×10^4 cm^{-3}, respectively. In the present study, ultrafine and nanoparticles generated from sintering processes (generally metal oxides) were considered as substances with a

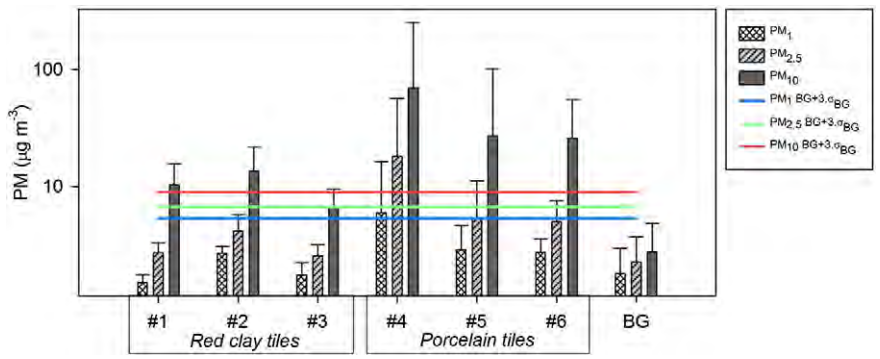

Fig. 8. Particle mass concentrations (PM) measured in the breathing zone for each of the materials analysed, as well as for background air. Mean values correspond to each sintering process, approximately 1.5 h. Error bars above the box indicate the standard deviation (σ). The solid blue, green and red horizontal line indicate the significance level of PM_1, $PM_{2.5}$ and PM_{10} concentrations during sintering in workplace air, respectively ($BG + 3 \cdot \sigma_{BG}$; Asbach et al., 2012).

Table 2
Background corrected 8 h-TWA particle number (N) and mass (PM) exposure concentrations obtained for each activity, and comparison with the SER nano-reference value (NRV) and the ACGIH threshold limit value (TLV).

Sintering activity	$N_{8\ h\text{-}TWA}$ (cm^{-3})	$NRV_{8\ h\text{-}TWA}$ (cm^{-3}) (SER, 2012)	$N_{8\ h\text{-}TWA}/NRV_{8\ h\text{-}TWA}$	$PM_{1\ 8\ h\text{-}TWA}$ ($\mu g\ m^{-3}$)	$PM_{2.5\ 8\ h\text{-}TWA}$ ($\mu g\ m^{-3}$)	$PM_{10\ 8\ h\text{-}TWA}$ ($\mu g\ m^{-3}$)	$TLV_{8\ h\text{-}TWA}$ ($\mu g\ m^{-3}$) ACGIH (2013)	$PM_{10\ 8\ h\text{-}TWA}/TLV_{8\ h\text{-}TWA}$
#1	3.7×10^5	4.0×10^4	9	<0.1	1.0	7.7	3.0×10^3	3×10^{-3}
#2	1.5×10^5		4	1.0	2.3	10.5		4×10^{-3}
#3	2.0×10^5		5	0.2	0.9	4.5		2×10^{-3}
#4	1.4×10^5		3	3.9	14.4	60.0		2×10^{-2}
#5	2.6×10^5		7	1.2	3.3	22.6		8×10^{-3}
#6	5.3×10^5		13	1.0	3.1	21.5		7×10^{-3}

density $< 6 \times 10^3$ kg m^{-3}. In general, only the pure metals have a density $> 6 \times 10^3$ kg m^{-3}(Van Broekhuizen, 2012).

In terms of *PM*, the only limits available are those established by the American Conference of Governmental Industrial Hygienists (ACGIH, 2013) and the Occupational Safety and Heath Administration (OSHA, 2006). These institutions set a permissible exposure limit (PEL; 8 h TWA) of 5 mg m^{-3} for the respirable fraction (PM_{10}) (OSHA, 2006) and of 3 mg m^{-3} (threshold limit value TLV, 8-hour TWA concentration) for respirable particles (PM_{10}) ACGIH (2013).

Table 2 represents the background-corrected 8 h-TWA worker exposure to *N* and *PM* concentrations (by Eq. (3)) during the sintering activities under study.

Considering that the workers were exposed to nanoparticle concentrations during a 7-hour working shift of sintering of each material and 1 h working during non-activity period, 8-hour TWA exposure *N* concentrations were in the range of 1.4×10^5 cm^{-3} and 5.3×10^5 cm^{-3}. This outcome exceeded the NRV established by the SER (2012) with a ratio ($N_{8\ h\text{-}TWA}/NRV_{8\ h\text{-}TWA}$) ranging from 3 to 13 (Table 2). In terms of mass, the 3 mg m^{-3}TLV for the total respirable fraction would not have been exceeded during any sintering condition given that the PM_{10} for 8 h TWA would be in the range of 5–60 μg m^{-3}.

3.6. Environmental release and filter efficiency

To mitigate the potential risk for ultrafine and nanoparticle release to the environment (ambient air), a filtration system (with a HEPA filter) was placed at the end of the exhaust conduct and before exhaust gases were released to outdoor air. The aim of this system was to remove particles originating from the tile sintering processes from the exhaust gas. However, at the time of the study, the facility managers had no specific data on the performance of the filtration system. Therefore, in order to test the effectiveness of the filtration system during tile sintering activity, particle number concentrations and size distribution were monitored before and after the HEPA filter (Table 3). The following formula was applied for the calculation of the filtration system efficiency:

$$\text{Efficiency of filtration system to reduce } N(\%) = \frac{N_{\text{before HEPA}} - N_{\text{after HEPA}}}{N_{\text{before HEPA}}} \times 100 \quad (4)$$

Table 3
Mean particle number concentration (N) measured before and after the HEPA filter, and calculated HEPA filtration efficiency for each sintering process.

Material	$N_{\text{mean before HEPA}}$ (cm^{-3})	$N_{\text{mean after HEPA}}$ (cm^{-3})	Efficiency* (%)
#1	2.0×10^6	1.0×10^5	95%
#2	2.1×10^6	7.4×10^4	96%
#3	2.5×10^6	8.5×10^4	97%
#4	1.1×10^6	5.9×10^4	95%
#5	2.8×10^6	1.6×10^5	94%
#6	2.8×10^6	1.1×10^5	96%

* Calculated by Eq. (4).

Results show that the mean and maximum *N* concentrations measured after the filtration system were lower than before the system by one or two orders of magnitude, implying a calculated system efficiency of 94–97% (Table 3). However, because of the high *N* emitted (in the order of 10^6 cm^{-3}), particle emissions to outdoor air in the order of mean 1.5-hour concentrations of 10^5 cm^{-3} were still detected (Table 3). The largest impacts on outdoor air were registered during porcelain sintering (1.1×10^5 cm^{-3}), and in particular for the porcelain with frit (material #5; 1.6×10^5 cm^{-3}) (Table 3). Because of rapid dilution processes it is not expected that this particle release would generate major environmental or health impacts in outdoor air.

Finally, filter efficiency seemed to be dependent on particle size. Fig. 9 shows the time series of the efficiency of the HEPA filtration system with regard to the mean particle diameters measured before and after the filtration system, for material #3 (red clay with frit and decoration). Similar results were obtained for the rest of the materials. Results evidence a clear inverse relationship between filtration efficiency and initial particle diameter (before the HEPA filter), with efficiency decreasing to <94% during the laser treatment periods when particle diameter increased (see Figs. 5 and 7). Conversely, during the thermal treatments (before and after laser incidence) particle size before the filtration system was close to the instrument's detection limit (10 nm) and higher efficiency values were registered (>97%).

As a result, the efficiency of the filtration system was successfully tested, evidencing a > 87% efficiency of *N* removal (on a 1-minute basis), mostly for nanoparticles <15 nm (Fig. 9). The lowest filter efficiency was detected for larger particles released during the laser treatment (~30 nm).

4. Conclusions

This study aimed to characterise particle formation and release mechanisms, and their impact on personal exposure and the environment during a tile sintering process using a high power CO_2 laser in an industrial up-scaling process. In addition, possible particle transformations during transport through the exhaust system and the effectiveness of the filtration system were also assessed.

Based on the experiments carried out, it was possible to conclude that new particle formation mechanisms from gaseous precursors occurred for both types of ceramic materials (red clay and porcelain) during the thermal treatment, independently of the laser treatment. The incidence of the laser seemed to inhibit new particle formation processes, possibly due to the sealing of the tile surface by the laser.

Ultrafine and nano-sized airborne particles were generated and emitted into workplace air during sintering process on a statistically significant level ($>BG + 3 \cdot \sigma_{BG}$). When comparing exposure levels to the exposure limits available in current regulations, according to SER (2012), exposure concentrations to ultrafine and nanoparticles generated in this workplace would exceed the nano-reference value (NRV) of 4×10^4 cm^{-3}, since their 8 h TWA was in the range of 1.4×10^5 cm^{-3} and 5.3×10^5 cm^{-3} (worst case scenario considering an equivalent workers exposure of 7 h working shift during sintering activity and 1 h working shift during non-activity period). In terms of mass, current regulations set a 3 mg m^{-3} TLV (8 h TWA; ACGIH, 2013) for the total

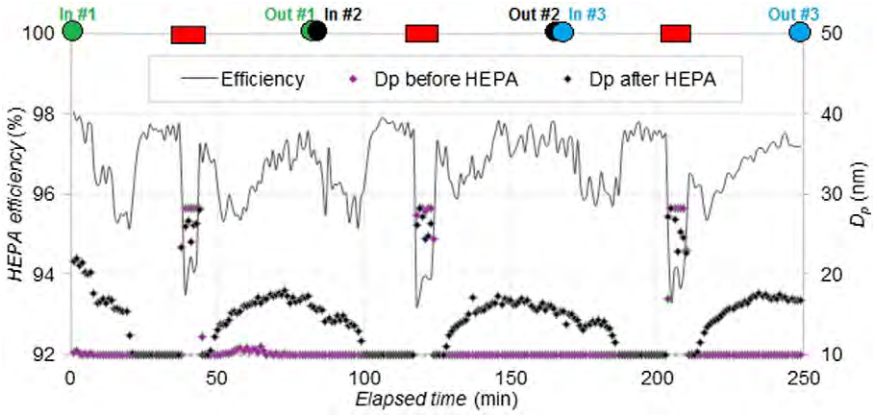

Fig. 9. Example of the efficiency of the HEPA filtration system (in %) as a function of particle diameter (range 10–700 nm) measured before and after the filtration system for each tile sintering process, for material #3 (red clay with frit and decoration). The laser period is shown as red rectangle and the entrance and exit of replicas #1, #2 and #3 are shown as green, black and blue circles, respectively. D_p: mean particle diameter (range 10–700 nm).

respirable fraction which would not have been exceeded during any sintering condition given that the PM_{10} for 8 h TWA would be in the range of 4.5–60 μg m^{-3}.

A potential risk of ultrafine and nanoparticle release to the outdoor air was identified, despite the mitigation measures in place (a HEPA filtration system). The efficiency of the filtration system was successfully tested, evidencing a >87% efficiency of *N* removal (on a 1-minute basis), mostly for nanoparticles <15 nm whereas it was slightly less efficient for larger particles released during the laser treatment (~30 nm).

Overall, the results from this study evidence the risk of occupational exposure to ultrafine and nanoparticles during high-energy laser processes in the ceramic facility under study. Although the results regarding exposures may not be extrapolated directly to real-world ceramic industrial facilities, this study may be taken as reference from a methodological perspective and with regard to the particle formation mechanisms described. In addition, our results could be representative of potential exposures in case of leaks in the process in industrial settings, when major nanoparticle releases would be expected. Hence, the development of mitigation strategies and systematic approaches toward better identifying the processes and/or materials are recommended to enable risk assessments and to reduce worker exposure.

Acknowledgements

This work was supported by the European Commission FP7 (FP7-PEOPLE-2012-ITN) Marie Curie ITN project no. 315760 (HEXACOMM) and by the Spanish MINECO (PCIN-2015-173-C02-01) under the frame of SIINN, the ERA-NET for a Safe Implementation of Innovative Nanoscience and Nanotechnology, through SIINN-ERANET project CERASAFE (id.:16). Additional support was provided by LIFE projects AIRUSE (LIFE11 ENV/ES/584), CERAMGLASS (LIFE11 ENV/ES/560) and LASERFIRING (LIFE09 ENV/ES/435).

Supplementary data

Supplementary data to this article can be found online at http://dx.doi.org/10.1016/j.scitotenv.2016.01.106.

References

ACGIH, 2013. Threshold Limit Values for Chemical Substances and Physical Agents and Biological Exposure Indices. American Conference of Governmental Industrial Hygienists.

Asbach, C., Kuhlbusch, T., Kaminski, H., Stahlmecke, B., Plitzko, S., Götz, U., Voetz, M., Kiesling, H.J., Dahmann, D., 2012. NanoGEM standard operation procedures for assessing exposure to nanomaterials, following a tiered approach. http://www.nanogem.de/cms/nanogem/upload/Veroeffentlichungen/nanoGEM_SOPs_Tiered_Approach.pdf.

Brouwer, D., Berges, M., Virji, M.A., Fransman, W., Bello, D., Hodson, L., Gabriel, S., Tielemans, E., 2012. Harmonization of measurement strategies for exposure to manufactured nano-objects; report of a workshop. Ann. Occup. Hyg. 56 (1), 1–9.

Brouwer, D., van Duuren-Stuurman, B., Berges, M., Jankowska, E., Bard, D., Mark, D., 2009. From workplace air measurement results toward estimates of exposure? Development of a strategy to assess exposure to manufactured nano-objects. J. Nanoparticle Res. 11 (8), 1867–1881. http://dx.doi.org/10.1007/s11051-009-9772-1.

Casasola, R., Rincón, J.M., Romero, M., 2012. Glass–ceramic glazes for ceramic tiles: a review. J. Mater. Sci. 47 (2), 553–582. http://dx.doi.org/10.1007/s10853-011-5981-y.

Celades, I., 2013. Caracterización física, química, mineralógica y morfológica del material particulado emitido por focos canalizados de la industria de baldosas y fritas cerámicas (PhD) Universitat Jaume I de Castellón, Castellón.

Cerame-Unie, 2012. The ceramic industry roadmap: paving the way to 2050. from http://cerameunie.eu/.

Chinchón, J.S., Querol, X., Fernández-Turiel, J.L., López-Soler, A., 1991. Environmental impact of mineral transformations undergone during coal combustion. Environ. Geol. Water Sci. 18 (1), 11–15. http://dx.doi.org/10.1007/bf01704573.

EC, 1998. Council directive 98/24/EC of 7 April 1998 on the protection of the health and safety of workers from the risks related to chemical agents at work (fourteenth individual directive within the meaning of article 16(1) of directive 89/391/EEC). OJ L 131, 5.5.1998, p. 11. Retrieved from http://eur-lex.europa.eu/LexUriServ/LexUriServ.do?uri=OJ:L:1998:131:0011:0023:EN:PDF.

Estepa, C., de la Fuente, G.F., Patent No. 200600560, 2006.

Fonseca, A.S., Viana, M., Querol, X., Moreno, N., de Francisco, I., Estepa, C., de la Fuente, G.F., 2015. Ultrafine and nanoparticle formation and emission mechanisms during laser processing of ceramic materials. J. Aerosol Sci. 88, 48–57. http://dx.doi.org/10.1016/j.jaerosci.2015.05.013.

de Francisco, I., Lennikov, V.V., Bea, J.A., Vegas, A., Carda, J.B., de la Fuente, G.F., 2011. In-situ laser synthesis of rare earth aluminate coatings in the system Ln–Al–O (Ln = Y, Gd). Solid State Sci. 13 (9), 1813–1819. http://dx.doi.org/10.1016/j.solidstatesciences.2011.07.013.

Gutiérrez Mora, F., Domínguez-Rodríguez, A., Lennikov, V.V., de la Fuente, G.F., 2009. Influence of thermal effects produced by laser treatment on the tribological behavior of porcelain ceramic tiles. Key Eng. Mater. 423, 41–46.

Hameri, K., Lahde, T., Hussein, T., Koivisto, J., Savolainen, K., 2009. Facing the key workplace challenge: assessing and preventing exposure to nanoparticles at source. Inhal. Toxicol. 1, 17–24.

Hansen, S.F., 2009. Regulation and Risk Assessment of Nanomaterials: Technical University of Denmark (DTU).

Heal, M.R., Kumar, P., Harrison, R.M., 2012. Particles, air quality, policy and health (10.1039/C2CS35076A) Chem. Soc. Rev. 41 (19), 6606–6630. http://dx.doi.org/10.1039/c2cs35076a.

Hoet, P.H., Bruske-Hohlfeld, I., Salata, O.V., 2004. Nanoparticles — known and unknown health risks [Journal article] J. Nanobiotechnol. 2 (1), 12.

Jaakkola, M.S., Sripaiboonkij, P., Jaakkola, J.J., 2011. Effects of occupational exposures and smoking on lung function in tile factory workers [Research Support, Non-US Gov't] Int. Arch. Occup. Environ. Health 84 (2), 151–158.

Jacobs, C.W.F., 1954. Opacifying crystalline phases present in zirconium-type glazes. J. Am. Ceram. Soc. 37 (5), 216–220. http://dx.doi.org/10.1111/j.1151-2916.1954.tb14026.x.

Kaminski, H., Beyer, M., Fissan, H., Asbach, C., Kuhlbusch, T.A.J., 2015. Measurements of nanoscale TiO2 and Al2O3 in industrial workplace environments — methodology and results. Aerosol Air Qual. Res. 15 (1), 129–141. http://dx.doi.org/10.4209/aaqr.2014.03.0065.

Kargar, F., Shahtaheri, S.J., Golbabaei, F., Barkhordari, A., Rahimi-Froushani, A., Khadem, M., 2013. Evaluation of occupational exposure of glazers of a ceramic industry to cobalt blue dye. Iran. J. Public Health 42 (8), 868–875.

Kulmala, M., Vehkamäki, H., Petäjä, T., Dal Maso, M., Lauri, A., Kerminen, V.M., Birmili, W., McMurry, P.H., 2004. Formation and growth rates of ultrafine atmospheric particles:

a review of observations. J. Aerosol Sci. 35 (2), 143–176. http://dx.doi.org/10.1016/j.jaerosci.2003.10.003.
Kumar, P., Fennell, P., Britter, R., 2008. Effect of wind direction and speed on the dispersion of nucleation and accumulation mode particles in an urban street canyon. Sci. Total Environ. 402 (1), 82–94. http://dx.doi.org/10.1016/j.scitotenv.2008.04.032.
Lahoz, R., de la Fuente, G.F., Pedra, J.M., Carda, J.B., 2011. Laser engraving of ceramic tiles. Int. J. Appl. Ceram. Technol. 8 (5), 1208–1217. http://dx.doi.org/10.1111/j.1744-7402.2010.02566.x.
Larrea, A., de la Fuente, G.F., Merino, R.I., Orera, V.M., 2002. ZrO_2–Al_2O_3 eutectic plates produced by laser zone melting. J. Eur. Ceram. Soc. 22 (2), 191–198. http://dx.doi.org/10.1016/S0955-2219(01)00279–5.
Lennikov, V.V., de Francisco, I., Bea, J.A., Estepa, L.C., de la Fuente, G.F., J.A.Garcia, 2010. Influencia de los efectos termicos inducidos por el tratamiento con laser CO_2 en la microestructura de baldosas ceramicas. In: Rodriguez y, R. (Ed.), Actas del XII Congreso Tratermat, pp. 373–379 (AIN ISBN: 978-84-693-6946-3).
Lennikov, V.V., Kazin, P.E., Tretyakov, Y.D., de la Fuente, G.F., 2004. Laser zone melting and texture formation in MgO-doped $Bi_{2.03}Sr_{1.93}Ca_{1.07}Cu_{2.05}O_{8+\delta}$. Z. Anorg. Allg. Chem. 630 (13–14), 2337–2342. http://dx.doi.org/10.1002/zaac.200400311.
Lennikov, V.V., Pedra, J.M., Gómez, J.J., de la Fuente, G.F., Carda, J.B., 2007. In situ synthesis of composite $MTiO_3$–Al_2O_3 coatings via laser zone melting. Solid State Sci. 9 (5), 404–409. http://dx.doi.org/10.1016/j.solidstatesciences.2007.03.013.
Methner, M., Hodson, L., Geraci, C., 2010. Nanoparticle Emission Assessment Technique (NEAT) for the identification and measurement of potential inhalation exposure to engineered nanomaterials—part A. J. Occup. Environ. Hyg. 7 (3), 127–132. http://dx.doi.org/10.1080/15459620903476355.
Minguillon, M.C., Monfort, E., Querol, X., Alastuey, A., Celades, I., Miro, J.V., 2009. Effect of ceramic industrial particulate emission control on key components of ambient PM_{10} [Research Support, Non-US Gov't] J. Environ. Manag. 90 (8), 2558–2567.
Mora, M., Diez, J.C., Lopez-Gascon, C.I., Martinez, E., de la Fuente, G.F., 2003. Laser textured Bi-2212 in planar geometries. IEEE Trans. Appl. Supercond. 13 (2), 3188–3191. http://dx.doi.org/10.1109/tasc.2003.812192.
Oberdorster, G., 2001. Pulmonary effects of inhaled ultrafine particles. Int. Arch. Occup. Environ. Health 74 (1), 1–8.
OECD, 2015. Harmonized Tiered Approach to Measure and Assess the Potential Exposure to Airborne Emissions of Engineered Nano-Objects and Their Agglomerates and Aggregates at Workplaces, Series on the Safety of Manufactured Nanomaterials No. 55, ENV/JM/MONO(2015)19. Environment Directorate, Organisation for Economic Co-operation and Development (OECD), Health and Safety Publications, Paris.
OSHA, 2006. 29 CFR 1910.1000. Z-3 Table.
Querol, X., Alastuey, A., Rodríguez, S., Plana, F., Ruiz, C.R., Cots, N., Massagué, G., Puig, O., 2001. PM_{10} and $PM_{2.5}$ source apportionment in the Barcelona Metropolitan Area, Catalonia, Spain. Atmos. Environ. 35, 6407–6419.
Ramachandran, G., Ostraat, M., Evans, D.E., Methner, M.M., O'Shaughnessy, P., D'Arcy, J., Geraci, C.L., Stevenson, E., Maynard, A., Rickabaugh, K., 2011. A strategy for assessing workplace exposures to nanomaterials. J. Occup. Environ. Hyg. 8 (11), 673–685.
Romero, M., Rincón, J.M., Acosta, A., 2003. Crystallisation of a zirconium-based glaze for ceramic tile coatings. J. Eur. Ceram. Soc. 23 (10), 1629–1635. http://dx.doi.org/10.1016/S0955-2219(02)00415–6.
de la Sánchez Campa, A.M., de la Rosa, J.D., González-Castanedo, Y., Fernández-Camacho, R., Alastuey, A., Querol, X., Pio, C., 2010. High concentrations of heavy metals in PM from ceramic factories of Southern Spain. Atmos. Res. 96 (4), 633–644. http://dx.doi.org/10.1016/j.atmosres.2010.02.011.
Schmoll, L.H., Elzey, S., Grassian, V.H., O'Shaughnessy, P.T., 2009. Nanoparticle aerosol generation methods from bulk powders for inhalation exposure studies. Nanotoxicology 3 (4), 265–275. http://dx.doi.org/10.3109/17435390903121931.
SER, 2012. Provisional Nano Reference Values for Engineered Nanomaterials, Advisory Report 12/01. Sociaal Economische Raad, Den Haag.
Trethowan, W.N., Burge, P.S., Rossiter, C.E., Harrington, J.M., Calvert, I.A., 1995. Study of the respiratory health of employees in seven European plants that manufacture ceramic fibres. Occup. Environ. Med. 52 (2), 97–104.
Van Broekhuizen, P., 2012. Nano Matters: Building Blocks for a Precautionary Approach. (PhD thesis Available at:) www.ivam.uva.nl/?nanomatters.
VCI, BAuA, RCI, B., IFA, IUTA, TUD, 2011. Tiered Approach to an Exposure Measurement and Assessment of Nanoscale Aerosols Released From Engineered Nanomaterials in Workplace Operations.
Viana, M., Rivas, I., Reche, C., Fonseca, A.S., Pérez, N., Querol, X., Alastuey, A., Álvarez-Pedrerol, M., Sunyer, J., 2015. Field comparison of portable and stationary instruments for outdoor urban air exposure assessments. Atmos. Environ. 123 (Part A), 220–228. http://dx.doi.org/10.1016/j.atmosenv.2015.10.076.
Voliotis, A., Bezantakos, S., Giamarelou, M., Valenti, M., Kumar, P., Biskos, G., 2014. Nanoparticle emissions from traditional pottery manufacturing [Research Support, Non-US Gov't] Environ. Sci.: Processes Impacts 16 (6), 1489–1494.
Weichenthal, S., 2012. Selected physiological effects of ultrafine particles in acute cardiovascular morbidity [Review] Environ. Res. 115, 26–36.